THE JOURNAL OF BIOLOGICAL CHEMISTRY
Vol. 276, No. 37, Issue of September 14, pp. 34913–34917, 2001
Printed in U.S.A.

Crystal Structure of Human Epidermal Growth Factor and Its Dimerization*

Received for publication, April 2, 2001, and in revised form, June 27, 2001
Published, JBC Papers in Press, July 3, 2001, DOI 10.1074/jbc.M102874200

He-Shu Lu‡, Ji-Jie Chai‡, Ming Li‡, Bing-Ren Huang§, Cun-Heng He§, and Ru-Chang Bi‡¶

From the ‡Institute of Biophysics, Chinese Academy of Sciences, Beijing 100101, China and the §Institute of Basic Medical Sciences, Chinese Academy of Medical Sciences and Peking Union Medical College, Beijing 100005, China

Epidermal growth factor (EGF) is a typical growth-stimulating peptide and functions by binding to specific cell-surface receptors and inducing dimerization of the receptors. Little is known about the molecular mechanism of EGF-induced dimerization of EGF receptors. The crystal structure of human EGF has been determined at pH 8.1. There are two human EGF molecules A and B in the asymmetric unit of the crystals, which form a potential dimer. Importantly, a number of residues known to be indispensable for EGF binding to its receptor are involved in the interface between the two EGF molecules, suggesting a crucial role of EGF dimerization in the EGF-induced dimerization of receptors. In addition, the crystal structure of EGF shares the main features of the NMR structure of mouse EGF determined at pH 2.0, but structural comparisons between different models have revealed new detailed features and properties of the EGF structure.

Human epidermal growth factor (hEGF)[1] is a polypeptide of 53 amino acids with three internal disulfide bridges. As a mitogen, it first binds with high affinity to specific cell-surface receptors and then induces their dimerization, which is essential for activating the tyrosine kinase in the receptor cytoplasmic domain, initiating a signal transduction that results in DNA synthesis and cell proliferation (1, 2). Although EGF is a typical growth-stimulating peptide, little is known about the molecular mechanism of EGF-induced receptor dimerization. EGF was found to exist predominantly as a monomeric species in solution, and based on analyses of binding of EGF to the extracellular domain of its receptor and of the resulting dimerization of the receptor, some models have been proposed for EGF-induced dimerization of receptors (3). However, all these models have yet to be verified by structural studies, the most important of which is the structural determination of the complex of EGF with its receptor.

Considerable attention has been paid to the structural elucidation of EGF for clarification of the structure/function relationship. Although the solution structure of EGF has been determined using NMR methods by several groups (4, 5, 6, 7, 8, 9), most of these NMR studies were performed at very acidic pH, where EGF completely loses its binding activity and biological potency (10). On the other hand, it has proved to be very difficult to grow good quality EGF crystals, despite the publication of a few relevant crystallization notes (11, 12). After numerous experiments to refine crystallization conditions, using a C-terminally truncated hEGF variant, we have obtained better quality EGF crystals in two different crystal forms at near physiological pH (13). Here we report the crystal structure of hEGF determined by the multiple isomorphous replacement method. There are two hEGF molecules in the asymmetric unit of the crystals that are in close end-to-end contact with each other. Analyses of the crystal structure and comparisons with NMR solution structures have revealed new details of the features and properties of the hEGF structure.

EXPERIMENTAL PROCEDURES

Materials—The C-terminally truncated hEGF was prepared as described (14). The *hEGF* gene encoding 51 amino acids was chemically synthesized based on preferred code usage in yeast. The gene was under the control of the alcohol oxidase promoter and the α-factor lead sequence including the 85-amino acid coding sequence. A multicopy insert was constructed as a part of the expression plasmid. The yeast *Pichia pastoris* was transformed by the expression plasmid, and a Mut^s His^+ cell line was screened. High cell density culture of the cell line was carried out, and the cells were induced with methyl alcohol. The human epidermal growth factor with biological activity was secreted into the medium and was purified through three chromatographic steps. The final yield was 100 mg per liter of cell culture with ~98% homogeneity. All columns were purchased from Amersham Pharmacia Biotech.

Crystallization and Data Collection—Crystallization of hEGF was performed as described (13). The hEGF concentration was about 50 mg/ml. After successive rounds of crystallization refinements using the hanging-drop vapor-diffusion method, larger hEGF crystals were grown from a solution containing 0.9 M $MgCl_2$, 3.5 mM CYMAL-3 (cyclohexylpropyl-b-D-maltoside) and 0.1 M Bicine (pH 8.1) at 291 K over a period of about two months. The hEGF crystals have a typical size of $0.4 \times 0.3 \times 0.3$ mm^3, and can eventually reach a size of $0.5 \times 0.5 \times 0.6$ mm^3. These crystals belong to the space group $P3_121$ ($a = b = 61.4$ Å, $c = 87.0$ Å). They could diffract x-ray to 3.0 Å resolution at Argonne Station of synchrotron radiation (Native 1 in Table I), and to 3.2 Å on a MarResearch IP detector, using Cu Kα x-ray from Rigaku RU-200 rotating-anode generator operating at 40 kV and 100 mA (Native 2). There are two EGF molecules (denoted by molecules A and B in the text) in the asymmetric unit of the trigonal crystals, giving a V_m of 3.82 $Å^3$/Da (15) and a corresponding solvent content of 67.6%. The weak diffractability of hEGF crystals may be related to the higher solvent content. The difficulty in growing good quality EGF crystals may be caused by the marked conformational flexibility of the EGF structure, which will be discussed in detail in the text.

Several heavy-atom derivatives were prepared by soaking the native crystals for 3 to 7 days at 293 K in storage solution containing an appropriate concentration of dissolved heavy atom compound. Intensity data for the heavy-atom derivatives were collected at room temperature on the MarResearch IP detector, using Cu Kα x-ray from Rigaku RU-200 rotating-anode generator operating at 40 kV and 100 mA. All

* This work was supported by the Natural Science Foundation of China and Chinese Manned Space Engineering. The costs of publication of this article were defrayed in part by the payment of page charges. This article must therefore be hereby marked "*advertisement*" in accordance with 18 U.S.C. Section 1734 solely to indicate this fact.

The atomic coordinates and structure factors (code 1JL9) have been deposited in the Protein Data Bank, Research Collaboratory for Structural Bioinformatics, Rutgers University, New Brunswick, NJ (http://www.rcsb.org/).

¶ To whom correspondence should be addressed. Tel.: 86-(10)-64889866; Fax: 86-(10)-64871293; E-mail: rcbi@iname.com.

[1] The abbreviations used are: hEGF, human epidermal growth factor; RMSD, root mean-squared deviation; MIR, multiple isomorphous replacement.

TABLE I
A summary of crystallography data

Data collection					
Data set[a]	Native1	Native2	K_2PtCl_6	$Hg(Ac)_2$	$UO_2(NO_3)_2$
Space group	$P3_121$	$P3_121$	$P3_121$	$P3_121$	$P3_121$
Resolution (Å)	100–3.0	30–3.2	20–4.4	20–4.0	20–4.3
Unit cell dimensions (Å)	$a = b = 61.43$	$a = b = 61.21$	$a = b = 60.86$	$a = b = 61.17$	$a = b = 61.03$
	$c = 87.04$	$c = 86.88$	$c = 86.76$	$c = 86.80$	$c = 87.24$
Number of molecules in asymmetric unit	2	2			
Observations/Unique	21097/4040	26521/3257	10710/1095	11950/1599	14001/1754
Overall completeness (%)	99.0	96.8	89.7	91.2	98.5
I/σ(I) (highest shell)	2.0	2.9	3.8	4.4	3.7
R_{merge} (%)[b]	10.4	10.5	10.9	9.3	12.3
Phasing data					
R_{cullis} (acentric/centric)[c]			0.78/0.70	0.82/0.79	0.93/0.93
Phasing power (acentric/centric)[d]			1.32/0.98	1.11/0.85	0.61/0.49
Occupancy			0.414	0.218	0.161
Refinement statistics					
Resolution (Å)	8.0–3.0				
R-factor[e]					
R_{cryst} (%)	23.1				
R_{free} (%)	28.3				
RMS deviations					
Bond lengths (Å)	0.007				
Bond angles (°)	1.193				

[a] Native1 is the data collected at Argonne Station; Native2, K_2PtCl_6, $Hg(Ac)_2$, $UO_2(NO_3)_2$ are data collected at Marresearch Image Plate and were used in structural determination with the MIR method.
[b] $R_{merge} = \Sigma|I_i - \langle I\rangle|/\Sigma|I_i|$, where I_i is the intensity of the ith observation and $\langle I\rangle$ is the mean intensity of the reflection, summed over all reflections.
[c] $R_{cullis} = \Sigma\|F_{PH} - F_P| - F_{Hcalc}|/\Sigma\|F_{PH}| - |F_P\|$, where F_P and F_{PH} are protein and heavy-atom structure factors, respectively, and F_{Hcalc} is the calculated heavy-atom structure factor.
[d] Phasing power $= \Sigma|F_{Hcalc}|/\Sigma\|F_{PH}| - |F_P\|$.
[e] R-factor $= \Sigma\|F_o| - |F_c\|/\Sigma|F_o|$, where F_o and F_c are the observed and calculated structure factors, respectively. R_{cryst} was calculated from the 90% of reflections used in refinement, and R_{free} was calculated from the remaining 10%.

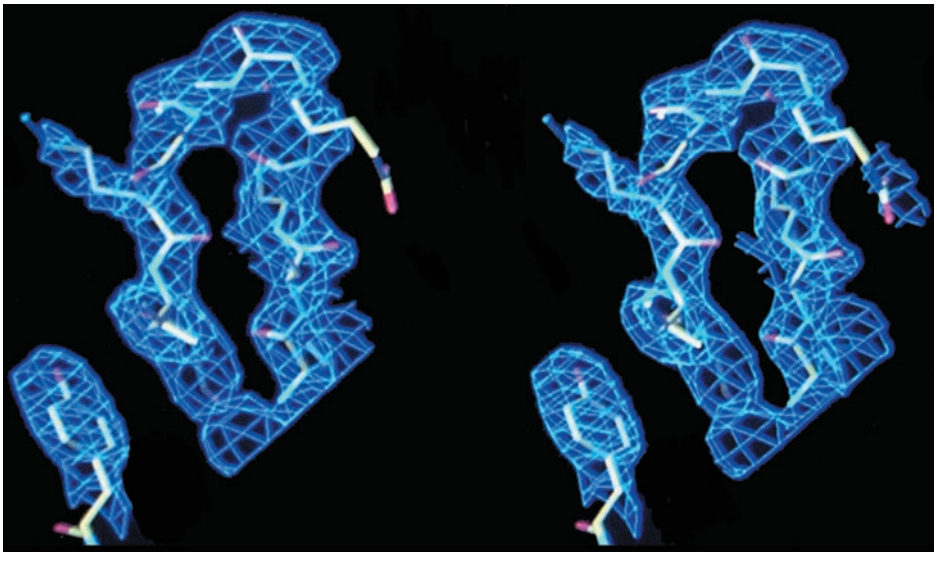

FIG. 1. **A $2F_o$-F_c electron density map surrounding residues 21–29 and Tyr[13].** It is displayed in stereo using TURBO-FRODO, computed at 3.0 Å resolution and contoured at 1.5σ. Carbon, oxygen, and nitrogen atoms are colored *yellow*, *red*, and *blue*, respectively.

diffraction data were processed with the programs DENZO and SCALEPACK (16).

Structure Determination and Refinement—Molecular replacement studies with NMR models of mouse EGF (mEGF) and several EGF-like domains as the search model were carried out with both data sets, Native 1 and Native 2. However, all these efforts failed, perhaps due to the difference between the NMR model and the crystal structure to be discussed in the text.

The multiple isomorphous replacement (MIR) was used to determine the hEGF structure, and all calculations were performed using corresponding programs in the CCP4 package (17) and Native 2 data. The heavy atoms in the derivative crystals were found by difference Patterson method and difference Fourier maps. Heavy atom positions were refined, and phases were calculated using the program MLPHARE with reflections of $F/\sigma(F)>2.0$, resulting in an initial figure of merit of 0.423 for data up to 4.0 Å. Solvent flattening and histogram matching improved the initial electron density using the program DM. It was finally determined at this point that there are two hEGF molecules in the asymmetric unit, and the boundaries between solvent and molecules were clearly shown in the electron density map.

Based on the availability of NMR structures, the phased translation function (18) was calculated to position the hEGF molecules in the unit cell. The relevant programs in CCP4 were used with the mean NMR structure of mEGF (PDB code 1EPG, Ref. 9), as the search model. Two possible model orientations obtained from the calculation of rotation function gave clear solutions of the phased translation function. Using these solutions, the initial model of hEGF crystal structure was built with program TURBO-FRODO (19) based on the electron density and resulted in a crystallographic R-factor of 49.4%.

The refinement and rebuilding of the hEGF structure were performed, mainly using simulated annealing, conjugate gradient minimization, and group B-factor refinement protocols of the program XPLOR (20) as well as the program TURBO-FRODO. Data between 8–3.3 Å with reflections of $F/\sigma(F)>2.0$ were used at the early stages of refinement, later extended to 3.0 Å, and 10% data were randomly kept aside for R_{free} calculation. Fourier maps with coefficients ($2F_o$-F_c) and (F_o-F_c) were calculated in each round. In addition, simulated annealing omit maps were computed for some ambiguous regions to trace the peptide

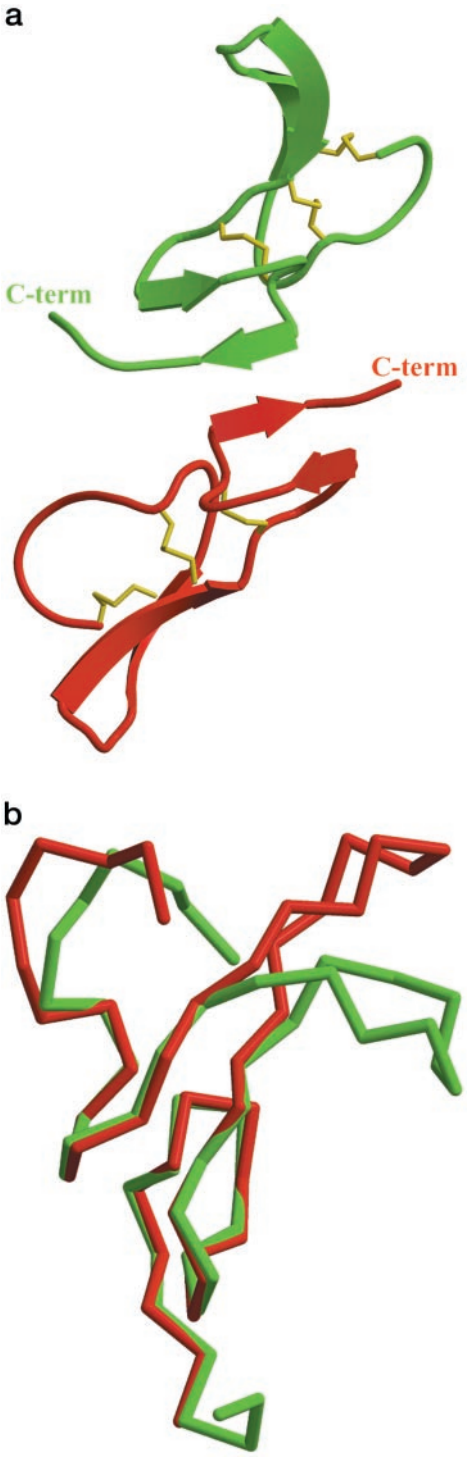

FIG. 2. **The two independent hEGF molecules A (in *red*) and B (in *green*).** *a*, related by a non-crystallographic 2-fold axis and form a potential dimer in the crystals. The three disulfide bridges, Cys^{6}–Cys^{20}, Cys^{14}–Cys^{31}, and Cys^{33}–Cys^{42} are shown in *yellow*. *b*, structural superposition of hEGF molecules A and B based on Cα atoms of rigid segments 13–21 and 30–47. The N-terminal segment (residues 1–12) and the residues 22–29 are adjacent to each other in the *upper* part of the figure. This figure was produced using MOLSCRIPT (33).

chain. During the final stages of refinement, 7 water molecules were inserted into the model. Due to the low resolution of the data, individual B-factor refinement was not carried out.

The final model was characterized by the program PROCHECK (21). Superposition between different models of the EGF structure was performed using LSQKAB in CCP4 package (17). The atomic coordinates of NMR structures of mEGF (9) were obtained from the Protein Data Bank under the accession code 1EPG and 1EPI, respectively.

RESULTS AND DISCUSSION

Model Quality—A summary of the structural analysis including data collection, phasing and refinement statistics for the hEGF crystals is presented in Table I. The values of R_{cryst} and R_{free} for the refined hEGF structure are 23.1 and 28.3%, respectively for the 8.0–3.0 Å data with $F>2\sigma(F)$. Amino acid residues 1–5 in both molecules A and B and the residues 48–51 in molecule A are disordered, as these regions are poorly defined in the electron density map. 98.6% of the remaining residues have appropriate backbone torsion angles in the most favorable and additionally allowed regions of the Ramachandran plot.

Except the two terminal segments, most main-chains in both hEGF molecules have well defined electron densities when contoured at 1σ level (Fig. 1). Most side chains are also unambiguously located in the density map, whereas some polar residues on the molecular surface have poor densities showing their conformational disorder to some extent. The three disulfide bridges, Cys^{6}–Cys^{20}, Cys^{14}–Cys^{31}, and Cys^{33}–Cys^{42}, are also located in clearly defined electron densities.

hEGF Structure—The crystal structure of hEGF (Fig. 2*a*) shares main features of the NMR solution structures available. It is a structure consisting of an N-domain (residues 1–32) and a C-domain (residues 33–53). The N-domain has an irregular N-terminal peptide segment with residues 1–12 and an anti-parallel β-sheet (residues 19–23/28–32). The C-domain contains a short anti-parallel β-sheet (residues 36–38/44–46) and a C-terminal segment with residues 48–53, which are probably disordered in isolation.

Despite structural similarity between molecules A and B in the asymmetric unit, large local differences are found in peptide segments 6–12, 22–29, and 48–51, respectively (Fig. 2*b*). The most obvious difference is located at the N-terminal residues up to residue Gly^{12}. Besides the disordered N-terminal segment with residues 1–5, residues 9–11 are well defined in molecule A, but not in molecule B. This difference may be caused by their different crystallographic environments. There are some intermolecular contacts between molecule A and a neighboring EGF molecule. They include three hydrogen bonds between residues Pro^{7}, Ser^{9} of molecule A, and Val^{35}, Cys^{33} of a neighboring molecule B in another asymmetric unit. However, there are no such kind of interactions between the N-terminal residues 6–11 of molecule B and any neighboring EGF molecules in the crystal. Another structural difference occurs at the surface turn with the residues 23–28 connecting the two anti-parallel β-strands of N-domain. The difference in the C-terminal peptide segment correlates with different exhibitions of electron densities for both molecules. In molecule B, residues 48–51 have clearly defined electron density, likely due to the intramolecular interactions between the residue 49 and other residues, such as the hydrogen bonds between Trp^{49}-O and Arg^{45}-NH1, Trp^{49}-N and Asp^{46}-O, whereas no electron density could be observed for residues 48–51 in molecule A.

Based on electron density map and structural comparisons between molecules A and B, several segments with rigid or flexible conformations could be defined in the EGF structure. Fig. 2*b* and Table II show that the rigid segments include residues 13–21 and 30–47. The RMSD for Cα atoms of these residues between molecules A and B is 0.517 Å. Another indication of inherent rigidity of these regions is that the average B-values of these residues are 22.14 and 26.04 $Å^2$ for main and side-chain atoms, respectively, compared with 30.07 and 36.59 $Å^2$ for the whole molecule. Two disulfide bridges, Cys^{14}–Cys^{31} and Cys^{33}–Cys^{42}, along with the highly conserved Gly^{18} and Gly^{39} play an important role for formation of the rigid region of the structure. The N-terminal segment (residues 1–12) and the

TABLE II
Cα atom RMS deviations calculated by least-square superposition between different models of the EGF structure

Models compared[a]	RMS Deviations (Å)				
	Residues 6–47	6–32	33–47	13–21, 30–32	13–21, 30–47
A & B	3.266	3.257	0.332	0.529	0.517 (0.252)[b]
A & N2	2.542	1.996	1.067	0.757	1.694 (2.751)
B & N2	3.952	3.312	1.078	0.702	1.754 (2.832)
A & N6.8	2.423	2.234	1.841	1.466	2.224 (6.497)
B & N6.8	3.769	3.235	1.799	1.558	2.313 (6.661)

[a] A = molecule A; B = molecule B; N6.8 = mouse NMR structure at pH 6.8; N2 = mouse NMR structure at pH 2.0.
[b] The values in parentheses are distances between Cα atoms of the residue Leu[47].

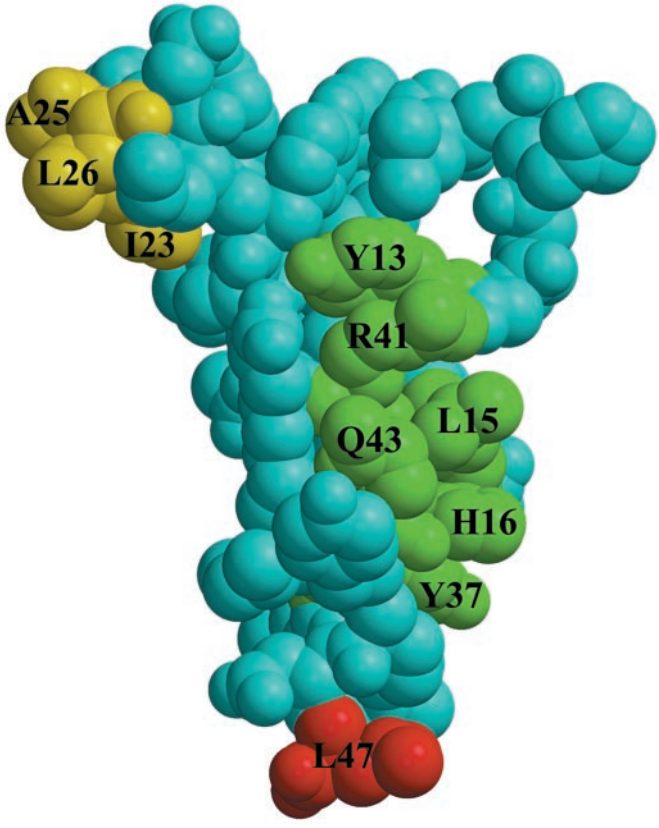

FIG. 3. **Space-filling model of the EGF molecule.** The figure shows the distribution of some surface residues known to be important for EGF binding to its receptor: Tyr[13], Leu[15], His[16], Tyr[37], Arg[41], Gln[43] (in *green*), Ile[23], Ala[25], Leu[26] (in *yellow*), and Leu[47] (in *red*).

residues 23–28 concerning the irregular β-turn between the two β-strands in the major β-sheet, which are adjacent to each other on the head of the EGF molecule, and the C-terminal segment (residues 48–53) belong to the flexible regions of the EGF structure.

Comparisons with NMR Structures—Comparisons by least-square superposition based on Cα atoms between the crystal and the NMR structures of EGF (9) were performed, and the results are shown in Table II. The whole molecule with residues 6–47 (without the disordered terminal segments), N-domain (6–32), and C-domain (33–47) were compared separately.

The comparisons of the crystal structure with the NMR structure at pH 2.0 have revealed that large structural differences are mainly located in the terminal segments, surface turns or loops, including residues 6–11, 24–27, 34–35, 39–40, and 45–47.

The flexible peptide segments (residues 1–12, 22–29, and 48–53) were excluded from more accurate comparisons between the NMR structure at pH 2.0 and the crystal structure. The overall RMSD based on the whole molecule (residues 13–21 and 30–47) for both molecules A and B are about 1.7 Å. However, the RMSD values based on a single domain are much lower, namely, about 0.7 Å for residues 13–21 and 30–32, and about 1.07 Å for residues 33–47 (Table II). This difference may result from a relative rotation of the two domains around a hinge residue between them. The structural variation might be caused by acidic pH, thus resulting in a very different arrangement of the C-terminal segment in the EGF solution structure. Compared with the positions in the crystal structures of molecules A and B, the Cα atom of Leu[47], a crucial residue for receptor binding (22), has moved by more than 2.75 Å in the NMR structure at pH 2.0.

Regarding the comparisons with the NMR structure at pH 6.8, despite the closer pH values, the RMSD values are larger than those calculated with the NMR structure at pH 2.0 (Table II). This implies that the NMR structure at pH 6.8 may not be sufficiently accurate due to the much lower number of distance constraints used compared with calculation of the pH 2.0 NMR structure (9).

Potential Dimer—Molecules A and B in the asymmetric unit are in close end-to-end contact and are related by a non-crystallographic 2-fold axis. The buried area between the two molecules is ~690 Å^2, which might be enough to maintain two such small molecules together to form a dimer under certain circumstances. The dimerization interface concerns the minor β-sheets from the C-domains of the two molecules, forming a short four-stranded anti-parallel β-sheet. The non-crystallographic 2-fold axis passes the center of this four-stranded β-sheet (Fig. 2*a*).

Leu[15], His[16], Tyr[37], Arg[41], Gln[43], Tyr[44], Arg[45], and Leu[47] from both hEGF molecules are involved in the intermolecular interface in the potential EGF dimer, although partial surfaces of side chains for some of these residues may be accessible. Besides the hydrogen bonds formed by atoms Gln[43]-O and Arg[45]-N in the four-stranded β-sheet, there are additional intermolecular hydrogen bonds between atoms His[16]-NE2 and Tyr[37]-OH in the dimer.

Conclusions and Implications—The crystal structure of hEGF determined at near physiological pH shares the main features of the NMR structure of mEGF determined at pH 2.0, but structural comparisons between different models revealed further details of the EGF structure. The structural differences of hEGF molecules A and B have shown detailed flexibility of the residues 22–29 in the hEGF structure. The structural comparison with the NMR structure at pH 2.0 may provide the first indication of the existence of relative movement between the N-domain and the C-domain of the EGF molecule.

The most important finding is that the dimerization of EGF molecules can occur under certain conditions. Notably, nearly all residues known to be crucial for EGF activity (23, 24), *i.e.* residues Leu[15], His[16], Tyr[37], Arg[41], Gln[43], and Leu[47] (Fig. 3), are involved in the intermolecular interface of the potential EGF dimer. It has been reported that the EGF-receptor complex contains two EGF molecules (3). Taking into account the

importance of ligand oligomers in the ligand-induced dimerization of receptors in some cases (25, 26, 27, 28), this potential EGF dimer might be biologically relevant and play a special role in the dimerization of EGF receptors. This suggestion is inconsistent with the models proposed by Lemmon *et al.* (3) in 1997, where any EGF aggregation is excluded from the molecular details of the EGF-induced dimerization of receptors. If the hypothesis concerning EGF dimerization is correct, and the consequence of the relative movement of the N- and C-terminal domains may impede formation of the potential EGF dimer; this may then account for the inactivation of EGF at acidic pH (10).

The important residues such as Leu^{15}, His^{16}, Tyr^{37}, Arg^{41}, Gln^{43}, and Leu^{47} are thought to be in the site of EGF binding to its receptor (23, 24). However, according to our hypothesis they are mainly involved in the intermolecular interface of the potential EGF dimer. So there must be other receptor binding sites in the EGF molecule, which are involved in formation of a bridge to the EGF receptor. Mutation and chimera studies of EGF have indicated that some residues, *e.g.* Ile^{23}, Ala^{25}, Leu^{26}, Ala^{30}, and Asn^{32} on the head of the EGF structure, may play an important role in the binding of EGF to its receptor (23, 29, 30). It is thought that they are mainly involved in providing a proper scaffold for the high affinity interaction between directly interacting amino acids and the receptor molecule (24, 31). As mentioned before (Fig. 2*b* and Table II), our structural analyses, in particular comparisons between the two molecules A and B of hEGF, have shown that the large conformational changes of these residues do not alter the type of scaffold in the EGF structure. So it is possible that the EGF head together with the variable segment containing residues 22–29 is directly involved in the interaction of EGF with its receptor. Support for this comes from a structural comparison of EGF with the 39-amino acid potato carboxypeptidase inhibitor. The latter is a low affinity EGF receptor antagonist. Its peptide segment residues 27–34 has a conformation closely similar to that of residues 22–29 in the NMR structure (32) or in the crystal structure of hEGF molecule A. The situation may resemble interferon-γ in receptor binding, where a flexible loop of interferon-γ is involved in the binding interface and undergoes a conformational change in the complex with the receptor (25). Therefore, important structural changes might occur in the flexible region involving residues 22–29 during EGF binding to its receptor.

In addition, if the above speculation is correct, this has implications for the heterodimerization of ErbB receptors, where there exists a 1:2 complex of ligand with receptors. It would suggest that the EGF dimerization might not play a role in the heterodimerization of ErbB receptors, and residues Leu^{15}, His^{16}, Tyr^{37}, Arg^{41}, Gln^{43}, Leu^{47} might play other roles in this case. Thus, further mutational studies of EGF are needed to show the different requirements for EGF-induced ErbB-1 homodimerization and for EGF-induced ErbB-1/ErbB-2 heterodimerization. However, in the process of heterodimeric formation, it could not be excluded that first a 2:2 ErbB-1 homodimer has to be formed, and subsequently ErbB-2 is involved, giving rise to a 2:4 complex, where ligand dimerization may be also of relevance for the formation of the heterodimeric receptor complex. To verify the above hypothesis, it is crucial to determine the structure of the complex of EGF with its receptor.

Acknowledgments—We thank Dr. Yu Luo and Prof. Ming Luo, Department of Microbiology, Center for Biophysical Science and Engineering, University of Alabama at Birmingham for collecting the 3.0 Å resolution data at Argonne Station. We thank Prof. E. J. J. Van Zoelen, Department of Cell Biology, University of Nijmegen, The Netherlands, for his helpful discussion about the molecular mechanism of ligand-induced dimerization of receptors. We also thank Prof. Yigong Shi, Department of Molecular Biology, Princeton University, for his reading the manuscript.

REFERENCES

1. Carpenter, G., King, L., and Cohen, S. (1978) *Nature* **276,** 409–410
2. Carpenter, G., and Cohen, S. (1990) *J. Biol. Chem.* **265,** 7709–7712
3. Lemmon, M. A., Bu, Z., Ladbury, J. E., Zhou, M., Pinchasi, D., Lax, I., Engelman, D. M., and Schlessinger, J. (1997) *EMBO J.* **16,** 281–294
4. Cooke, R. M., Wilkinson, A. J., Baron, M., Pastore, A., Tappin, M. J., Campbell, I. D., Gregory, H., and Sheard, B. (1987) *Nature* **327,** 339–341
5. Montelione, G. T., Wüthrich, K., Nice, E. C., Burgess, A. W., and Scheraga, H. A. (1987) *Proc. Natl. Acad. Sci. U. S. A.* **84,** 5226–5230
6. Montelione, G. T., Wuthrich, K., Burgess, A. W., Nice, E. C., Wagner, G., Gibson, K. D., and Scheraga, H. A. (1992) *Biochemistry* **31,** 236–249
7. Kohda, D., Go, N., Hayashi, K., and Inagaki, F. (1988) *J. Biochem.* **103,** 741–743
8. Hommel, U., Harvey, T. S., Driscoll, P. C., and Campbell, I. D. (1992) *J. Mol. Biol.* **227,** 271–282
9. Kohda, D., and Inagaki, F. (1992) *Biochemistry* **31,** 11928–11939
10. Massagué, J. (1983) *J. Biol. Chem.* **258,** 13614–13620
11. Higuchi, Y., Morimoto, Y., Horinaka, A., and Yasuoka, N. (1988) *J. Biochem.* **103,** 905–906
12. Degenhardt, M., Weber, W., Eschenburg, S., Dierks, K., Funari, S. S., Rapp, G., and Betzel, C. (1998) *Acta Crystallogr. Series D* **54,** 999–1001
13. Chai, J. J., Li, M., Huang, B. R., Luo, Y., Luo, M., Bi, R.-C., He, C.-H. (2000) *Acta Crystallogr. Series D* **56,** 62–63
14. Huang, B. R., Cai, L. W., Liao, H. T., Tang, S. X., and Zhou, H. T. (1998) *Chinese J. Biochem. Mol. Biol.* **14,** 512–517
15. Matthews, B. W. (1968) *J. Mol. Biol.* **33,** 491–497
16. Otwinowski, Z. (1993) *Oscillation Data Reduction Program in Data Collection and Processing* (Sawyer, L., Isaacs, N., and Bailey, S., eds) pp. 56–62, Daresbury Laboratory, Warrington UK
17. Collaborative Computational Project, Number 4 (1994) *Acta Crystallogr. Series D,* **50,** 760–763
18. Colman, P. M., Fehlhammer, and Bartels, K. (1976) *Crystallographic Computing Techniques,* p. 248, Munksgaard, Copenhagen
19. Jones, T. A. (1985) *Methods Enzymol.* **115,** 157–171
20. Brunger, A. T., Kuriyan, J., and Karplus, M. (1987) *Science* **235,** 458–460
21. Laskowski, R. A., Macarthur, M. W., Moss, D. S., and Thornton, J. M. (1993) *J. Appl. Crystallogr.* **26,** 283–291
22. Matsunami, R. K., Yette, M. L., and Stevens, A. (1991) *J. Cell. Biochem.* **46,** 242–249
23. Groenen, L. C., Nice, E. C., and Burgess, A. W. (1994) *Growth factor* **11,** 235–257
24. Van Zoelen, E. J. J., Stortelers, C., Lenferink, A. E. G., and Van De Poll, M. L. M. (2000) *Vitam. Horm.* **59,** 99–131
25. Walter, M. R., Windsor, W. T., Nagabhushan, T. L., Lundell, D. J., Lunn, C. A., Zauodny, P. J., and Narula, S. K. (1995) *Nature* **376,** 230–235
26. Banner, D. W., D'Arcy, A., Janes, W., Gentz, R., Schoenfeld, H. J., Broger, C., Loetscher, H., and Lesslauer, W. (1993) *Cell* **73,** 431–445
27. Philo, J., Talvenheimo, J., Wen, J., Rosenfeld, R., Welcher, A., and Arakawa, T. (1994) *J. Biol. Chem.* **269,** 27840–27846
28. Spivak-Kroizman, T., Lemmon, M. A., Dikic, I., Ladbury, J. E., Pinchasi, D., Huang, J., Jaye, M., Crumley, G., Schlessinger, J., and Lax, I. (1994) *Cell* **79,** 1015–1024
29. Richter, A., Drummond, D. R., MacGarvie, J., Puddicombe, S. M., Chamberlin, S. G., and Davies, D. E. (1995) *J. Biol. Chem.* **270,** 1612–1616
30. Van de Poll, M. L., Van Vugt, M. J., Lenferink, A. E., and Van Zoelen, E. J. (1997) *Biochemistry* **36,** 7425–7431
31. Campbell, I. D., Cooke, R. M., Baron, M., Harvey, T. S., and Tappin, M. J. (1989) *Prog. Growth Factor Res.* **1,** 13–22
32. Blanco-Aparicio, C., Molina, M. A., Fernandez-Salas, E., Frazier, M. L., Mas, J. M., Querol, E., Aviles, F. X., and De Llorens, R. (1998) *J. Biol. Chem.* **273,** 12370–12377
33. Kraulis, P. J. (1993) *J. Appl. Crystallogr.* **26,** 283–290